Chapter 4

Online Monitoring of Voltage Stability Margin Using PMU Measurements

4.1 Introduction

Voltage stability has been considered as an important threat against secure operation of power system [1]. Several incidences of voltage instability initiated grid failures have been observed in different parts of the world [78]. Various approaches for offline estimation of voltage stability have been well documented [111]. Offline assessment of voltage stability is quite useful in advance planning of preventive and corrective measures against instability. However, secure operation of a system in real time framework requires its online monitoring against instability. A forecasting-aided state estimation has been proposed for online monitoring of voltage stability [28]. Online assessment of voltage stability margin based on available reactive power reserve has been suggested [112]. Yiwei Qiu et. al. proposed parametric polynomial approximation of static voltage stability region boundaries based on Galerkin method and, suggested real time determination of left and right eigen vectors associated with zero eigen value at the estimated saddle-node-bifurcation space for online monitoring and control of voltage stability [110].

With advancement in wide-area monitoring system (WAMS) technology, online monitoring of voltage stability through time stamped measurements by Phasor Measurement Units (PMUs) seems possible. In comparison to Supervisory Control and Data Acquisition (SCADA) System the utilization of PMUs shows improved decision making and operation [113]. Many researchers proposed online monitoring of voltage

stability margin by obtaining Thevenin's equivalence of network across a critical load bus based on real time measurements by PMUs. Online estimation of voltage stability margin through matching of critical load impedance with PMU measurements based Thevenin's impedance of the rest of the network has been proposed [102], [114-116]. Representation of whole network connected across a critical load bus may be suitable for voltage stability monitoring of radial networks. However, interconnected power system may have a critical area comprising of a set of critical load buses prone to voltage collapse. Thevenin's equivalent of critical load area based on PMU measurements at its surrounding buses has been proposed [117], [118]. All the buses in the critical load area have been merged to replace these by a fictitious load bus. A critical load area is fed by multiple tie-lines, in general. Some of these may have over flows that may lead to voltage instability in the area. Replacing all the buses in the area with a single equivalent bus merges all the tie-lines too into a fictitious equivalent tie-line. Therefore, tie-lines of original network having overflows and hence being responsible for instability cannot be detected. In order to address this issue, online monitoring of voltage stability margin of a load area based on tie-line flows has been proposed [119]. Tie-line flows have been obtained through phasor measurements performed by PMUs placed at boundary buses of the critical load area. However, critical load areas are dependent upon operating conditions and topology of the network. Change of network topology due to occurrence of contingencies may lead to emergence of new critical load areas where PMUs are not placed.

Distributed linear algorithm has been proposed for online computation of voltage stability proximity indices (VCPI) based on local phasor measurements performed at all the load buses [120]. PMU measurements based online monitoring of

critical buses using *Q-V* (reactive power - voltage magnitude) and *P-Θ* (real power – voltage angle) sensitivities has been proposed [105]. However, assumption of *Q-Θ* and *P-V* decoupling are not valid near nose point. A normalized *P*-index has been proposed for online monitoring of voltage stability using phasor measurements [121]. However, *P*-index has been developed assuming constant power factor under increased demand which is not valid for real time systems.

Online monitoring of voltage stability based on Thevenin's equivalent of the network [102], [114]-[119], as well as sensitivity based real time estimation of voltage stability margin [105], [120]-[121] may fail to produce satisfactory results in case of large disturbances due to highly non-linear behavior of power systems. An Artificial Neural Network (ANN) based monitoring of voltage stability based on phasor measurements has been proposed [43]. Proper training of ANN is still a challenge. Enhanced-Online-Random-Forest (EORF) model has been proposed based on voltage phasor measurements for online monitoring of voltage stability [122]. EORF model updates voltage stability information under change in operating conditions/network topology using fresh PMU measurements at important load buses. EORF model may lead sometimes to erroneous estimation of voltage stability margin due to non-consideration of voltage phasor information of remaining buses. A general method to adjust loads at the receiving end has been applied to determine the proximity to voltage collapse [123]. Here, it is concluded that the intermediate load adjustment improves the accuracy of the indices. In this, the PMUs are not placed optimally in the system. In most of the research the statistical information obtained from PMUs has not actionably used to improve the voltage stability. In [124], the new method has been

suggested that gauges and improves the voltage stability of a system using statistical data obtained from PMUs.

In this chapter, real time determination of nose curve of all the load buses based on three successive PMU measurements and pseudo-measurements is performed. Minimum out of maximum loadability of all the load buses has been considered as the loading margin of the system. Voltage stability information is updated with new PMU measurements obtained. Thus, proposed approach is capable of monitoring voltage stability of real time systems as change in system operating conditions and network topology is considered by updated PMU measurements performed at regular intervals. PMUs have been optimally placed in the system based on result of binary integer linear programming ensuring full network observability even in case of loss of few PMUs under contingencies.

4.2 Methodology

Proposed approach of online monitoring of voltage stability margin using phasor measurements is presented below:

Real power demand (P_{D_i}) versus voltage magnitude V_i curve (*P*-*V* curve) of bus-*i* (shown in Fig.4.1) may be approximately obtained by solution of quadratic equation,

$$P_{D_i} = a_{1i}V_i^2 + a_{2i}V_i + a_{3i} \qquad (4.1)$$

where, a_{1i} , a_{2i} and a_{3i} are constants

Differentiating P_{D_i} with respect to V_i ,

$$\frac{dP_{D_i}}{dV_i} = 2a_{1i}V_i + a_{2i} \tag{4.2}$$

At nose point of *P*-*V* curve, $\frac{dP_{D_i}}{dV_i} = 0$. Therefore, from (4.2),

$$V_i^{np} = -\frac{a_{2i}}{2a_{1i}} \tag{4.3}$$

where, V_i^{np} = voltage magnitude of bus-*i* at the nose point of *P*-*V* curve (shown in Fig.4.1).

From (4.1) and (4.3),

$$P_{D_i}^{n} = -\frac{a_{2i}^2}{4a_{1i}} + a_{3i} \tag{4.4}$$

where, $P_{D_i}^{n}$ = Real power demand of bus-*i* at the nose point of *P*-*V* curve (shown in Fig.4.1).

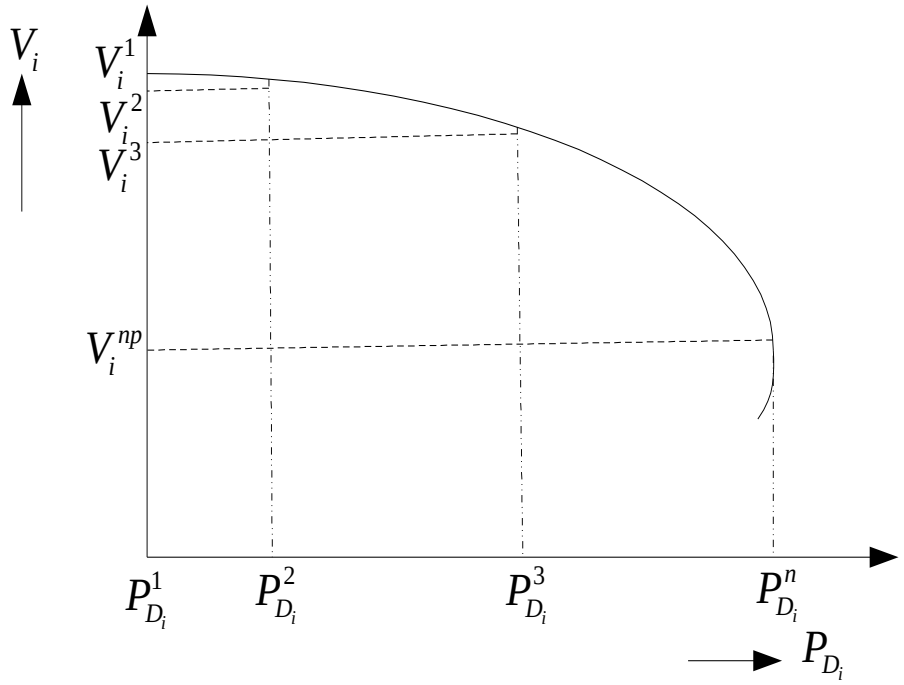

Fig.4.1. *P*-*V* curve of bus-*i*

Reactive power demand (Q_{D_i}) versus voltage magnitude (V_i) curve (Q-V curve) of bus-*i* (shown in Fig.4.2) may be approximately obtained by solution of quadratic equation,

$$Q_{D_i} = b_{1i}V_i^2 + b_{2i}V_i + b_{3i} \tag{4.5}$$

where, b_{1i}, b_{2i} and b_{3i} are constants.

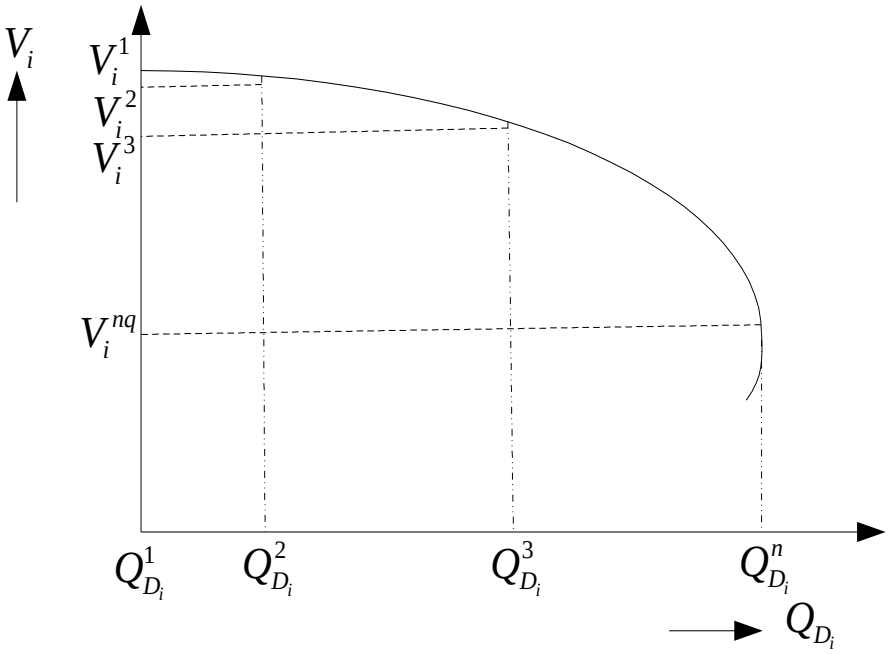

Fig.4.2. *Q*-*V* curve of bus-*i*

Differentiating Q_{D_i} with respect to V_i,

$$\frac{dQ_{D_i}}{dV_i} = 2b_{1i}V_i + b_{2i} \tag{4.6}$$

At the nose point of Q-V curve, $\frac{dQ_{D_i}}{dV_i} = 0$, Therefore, from (4.6),

$$V_i^{nq} = -\frac{b_{2i}}{2b_{1i}} \tag{4.7}$$

where, V_i^{nq} = voltage magnitude of bus-*i* at the nose point of *Q*-*V* curve (shown in Fig.4.2).

From (4.5) and (4.7),

$$Q_{D_i}^n = -\frac{b_{2i}^2}{4b_{1i}} + b_{3i} \tag{4.8}$$

where, $Q_{D_i}^n$ = Reactive power demand of bus-*i* at the nose point of *Q*-*V* curve (shown in Fig.4.2).

Constants a_{1i}, a_{2i} and a_{3i} were obtained by solution of equations:

$$P_{D_i}^1 = a_{1i}(V_i^1)^2 + a_{2i}V_i^1 + a_{3i} \tag{4.9}$$

$$P_{D_i}^2 = a_{1i}(V_i^2)^2 + a_{2i}V_i^2 + a_{3i} \tag{4.10}$$

$$P_{D_i}^3 = a_{1i}(V_i^3)^2 + a_{2i}V_i^3 + a_{3i} \tag{4.11}$$

where, V_i^1, V_i^2, V_i^3 (shown in Fig.4.1 and in Fig.4.2) correspond to voltage magnitude of bus-*i* at operating points 1, 2 and 3, respectively, and $P_{D_i}^1$, $P_{D_i}^2$ and $P_{D_i}^3$ (shown in Fig.4.1) correspond to real power demand of bus-*i* at operating points 1, 2 and 3, respectively.

Evaluated constants a_{1i}, a_{2i} and a_{3i} were used to find real power loading margin of bus-*i* using (4.4).

Constants b_{1i}, b_{2i} and b_{3i} are obtained by solution of equations:

$$Q_{D_i}^1 = b_{1i}(V_i^1)^2 + b_{2i}V_i^1 + b_{3i} \quad (4.12)$$

$$Q_{D_i}^2 = b_{1i}(V_i^2)^2 + b_{2i}V_i^2 + b_{3i} \quad (4.13)$$

$$Q_{D_i}^3 = b_{1i}(V_i^3)^2 + b_{2i}V_i^3 + b_{3i} \quad (4.14)$$

where, $Q_{D_i}^1$, $Q_{D_i}^2$ and $Q_{D_i}^3$ (shown in Fig.4.2) correspond to reactive power demand of bus-*i* at operating points 1, 2 and 3, respectively.

Evaluated constants b_{1i}, b_{2i} and b_{3i} were used to find reactive power loading margin of bus-*i* using (4.8).

Constants a_{1i}, a_{2i}, a_{3i}, b_{1i}, b_{2i} and b_{3i} for each of the load buses were evaluated using voltage magnitude, real power demand and reactive power demand obtained by PMU measurements/pseudo measurements performed at operating points 1, 2 and 3, respectively. Evaluated constants predict real power loading margin as well as reactive power loading margin of each bus using (4.4) and (4.8), respectively. Minimum out of maximum real power loadability of all the load buses present in the system is considered as real power loading margin of the system, and corresponding bus was considered as the most critical bus based on real power loading margin. Minimum out of maximum reactive power loadability of all the load buses present in the system was considered as reactive power loading margin of the system, and corresponding bus was considered as the most critical bus based on reactive power loading margin criterion. A flow chart for finding loading margin as well as most critical bus based on PMU measurements is shown in Fig.4.3. Since, loading margin of a real time system keeps on changing with change in operating conditions; it is proposed to update loading margin as well as most critical bus information based on new PMU measurements obtained, at regular intervals. Flowchart shown in Fig.4.3 assumes very high initial

loading margin of 10,000 MW and 10,000 MVAR, respectively, keeping in mind such values to be higher than loading margin of any of the load buses present in the system, and keeps on reducing these till real power loading margin as well as reactive power loading margin of the most critical bus are obtained.

Pseudo measurements were performed using network observability rules mentioned in Section 2.3.

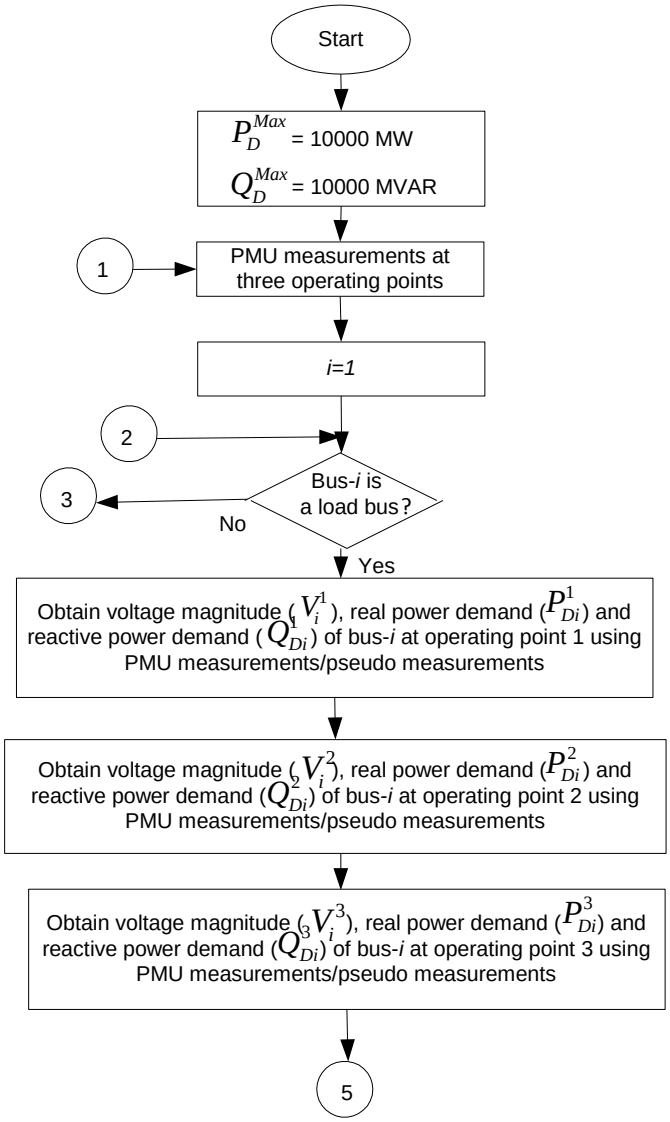

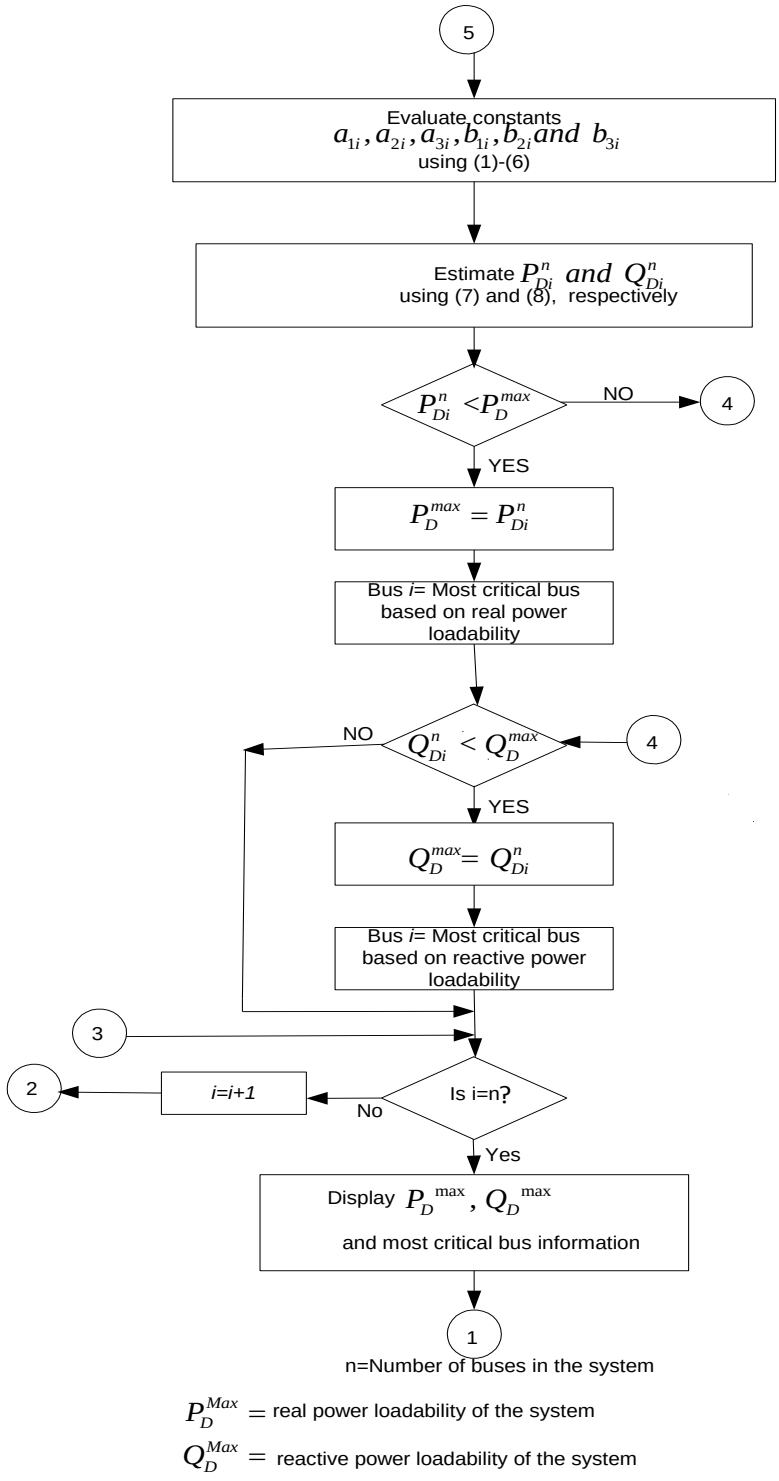

Figure 4.3: Flowchart for determining loading margin of system using proposed approach

4.3 Case Studies

Proposed approach of online monitoring of voltage stability margin was tested on IEEE 14-bus system, New England 39-bus system and 246-bus Northern Region Power Grid (NRPG) system of India with the help of Power System Analysis Toolbox (PSAT) software. Details of three systems are presented in Appendix-A, Appendix-B, Appendix-C, respectively. Simulation results obtained on three systems are presented below:

4.3.1 IEEE 14-Bus System

Voltage magnitude, real power demand and reactive power demand of all the load buses were obtained at three operating points (viz. points 1, 2 and 3, respectively) using combination of PMU measurements and pseudo measurements for the system intact case. Constants $a_{1i,}$ a_{2i} and a_{3i} were calculated using (4.9), (4.10) and (4.11) for each of the load buses. Evaluated constants were used to find nose point real power demand ($P_{D_i}^n$) of each load bus using (4.4). Minimum out of nose point real power demand of all the load buses was considered as real power loading margin P_D^{Max} of the intact system, and bus having minimum $P_{D_i}^n$ value was considered as the most critical bus requiring attention as far as system real power loadability is concerned. In order to update loading margin information under change in operating scenario, PMU measurements as well as pseudo measurements obtained at three operating points under all the single line outage cases were used for evaluation of updated $a_{1i,}$ $a_{2i,}$ a_{3i} for all the load buses, and new P_D^{Max} were calculated under these conditions using flow chart shown in Fig.4.3. Measured voltage magnitude and real power demand of the

most critical bus at the three operating points, P_D^{Max} calculated using proposed approach and real power loadability based most critical bus number have been shown in Table 4.1 for the system intact case and few critical contingency cases. In order to validate real power loading margin obtained by proposed approach, real power demand versus voltage magnitude curve (*P*-*V* curve) of most critical bus was plotted using continuation power flow (CPF) method [10] for the system intact case and all the single line outage cases. For obtaining *P*-*V* curve of the most critical bus using CPF method, its real power demand P_{D_j} was varied as per following:

$$P_{Dj} = P_{D_j}^1(1 + \lambda_{jp}) \qquad (4.15)$$

where, λ_{jp}= fraction of real power demand increase at bus-*j*

Real power loading margin (P_D^{Max}) of the most critical bus obtained by CPF method (real power demand at the nose point of its *P*-*V* curve) have also been shown in Table 4.1 for the system intact case and few critical contingency cases. It is observed from Table 4.1 that real power loading margin obtained by proposed approach closely matches with real power loading margin found by continuation power flow method.

Table 4.1: Real power loading margin under critical contingencies (IEEE 14-bus system)

C.C.	M.C.B.	Point 1		Point 2		Point 3		P_D^{Max} (MW)	
		V_j^1 (p.u.)	$P_{D_j}^1$ (MW)	V_j^2 (p.u.)	$P_{D_j}^2$ (MW)	V_j^3 (p.u.)	$P_{D_j}^3$ (MW)	P.A.	CPF
Intact	5	1.03	7.6	0.96	36.16	0.90	37.09	39.44	40.20
1-2	5	1.03	7.6	0.95	17.71	0.91	16.26	17.78	16.49
2-3	4	1.03	47.8	0.95	177.82	0.90	187.85	189.77	188.33
2-4	5	1.03	7.6	0.96	30.40	0.90	30.86	32.76	32.91
1-5	5	1.02	7.6	0.95	37.32	0.92	34.50	37.39	34.50
2-5	5	1.02	7.6	0.95	33.14	0.90	33.21	35.64	35.26

C.C. = critical contingency, M.C.B. = most critical bus, P.A. = proposed approach

P-V curve of bus 4 (most critical bus) obtained by proposed quadratic fitting of nose curves using PMU measurements/pseudo measurements at three operating points as well as continuation power flow based *P-V* curve of same bus have been shown in Fig.4.4 for the outage of line 2-4. It is observed from Fig.4.4 that nose point real power loadability obtained by proposed approach closely matches with real power loading margin of the bus obtained by continuation power flow method.

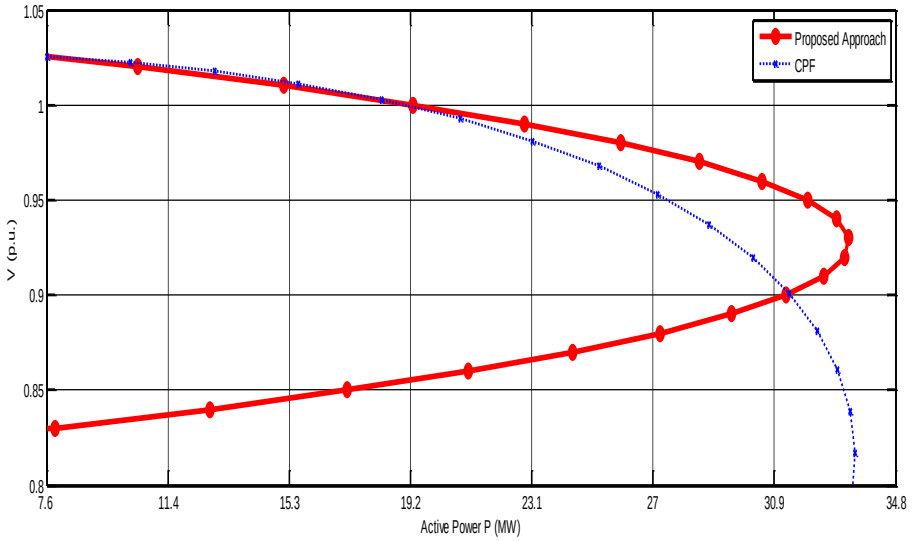

Figure 4.4: *P-V* curve of critical bus 5 obtained using proposed quadratic curve fitting method and by CPF method for line outage 2-4.

Constants b_{1i}, b_{2i} and b_{3i} were calculated for each of the load buses using (4.12), (4.13) and (4.14) for the system intact case and all the single line outage cases using PMU measurements/pseudo measurements. Evaluated constants were utilized to determine nose point reactive power demand, $Q_{D_i}^n$ of each bus using (4.8). Minimum out of nose point reactive power demand ($Q_{D_i}^n$) of all the load buses was considered as reactive power loading margin Q_D^{Max} of the system, and bus having minimum $Q_{D_i}^n$ value was considered as most critical bus requiring attention as for as reactive power loading margin is concerned. In order to validate reactive power loading margin obtained by proposed approach, reactive power demand versus voltage magnitude curve (*Q-V* curve) of the most critical bus was obtained by CPF method for the system intact case and all the single line outage cases. For obtaining *Q-V* curve of the most critical bus using CPF method, its reactive power demand was varied using:

$$Q_{D_j} = Q_{D_j}^1 (1 + \lambda_{jq}) \quad (4.16)$$

where, λ_{jq}= fraction of reactive power demand increase at bus-*j*

Measured voltage magnitude and reactive power demand of most critical bus at three operating points, reactive power loading margin (Q_D^{Max}) obtained by proposed approach as well as by CPF method have been shown in Table 4.2, for the system intact case and few critical contingency cases. Reactive power loadability based most critical bus number has also been shown in Table 4.2 for all these cases. It is observed from Table 4.2 that Q_D^{Max} obtained by proposed approach closely matches with Q_D^{Max} obtained by CPF method.

Table 4.2: Reactive power loading margin under critical contingencies (IEEE 14-bus system)

C.C.	M.C.B.	Point 1		Point 2		Point 3		Q_D^{Max} (MVAR)	
		V_j^1 (p.u.)	$Q_{D_j}^1$ (MVAR)	V_j^2 (p.u.)	$Q_{D_j}^2$ (MVAR)	V_j^3 (p.u.)	$Q_{D_j}^3$ (MVAR)	P.A.	CPF
Intact	5	1.03	0.32	0.96	3.81	0.90	7.81	0.85	0.86
1-2	5	1.03	0.32	0.95	1.86	0.91	3.42	0.56	0.54
2-3	4	1.03	0.78	0.95	7.25	0.90	15.33	3.10	3.07
6-13	13	1.01	1.16	0.95	3.2	0.91	6.50	5.57	6.04
9-14	14	1.02	1.0	0.96	3.93	0.92	7.26	4.68	5.22
9-10	10	1.02	1.16	0.96	3.49	0.91	6.99	5.64	6.10

C.C. = critical contingency, M.C.B. = most critical bus, P.A. = proposed approach

Q-V curve of bus 4 (most critical bus) obtained by proposed quadratic curve fitting of nose curves using PMU measurements/pseudo measurements obtained at three operating points as well as CPF based *Q-V* curve of same bus have been shown in Fig.4.5 for the outage of line 2-3. It is observed from Fig.4.5 that nose point reactive power loadability of bus 4 obtained by proposed approach closely matches with CPF based nose point reactive power demand.

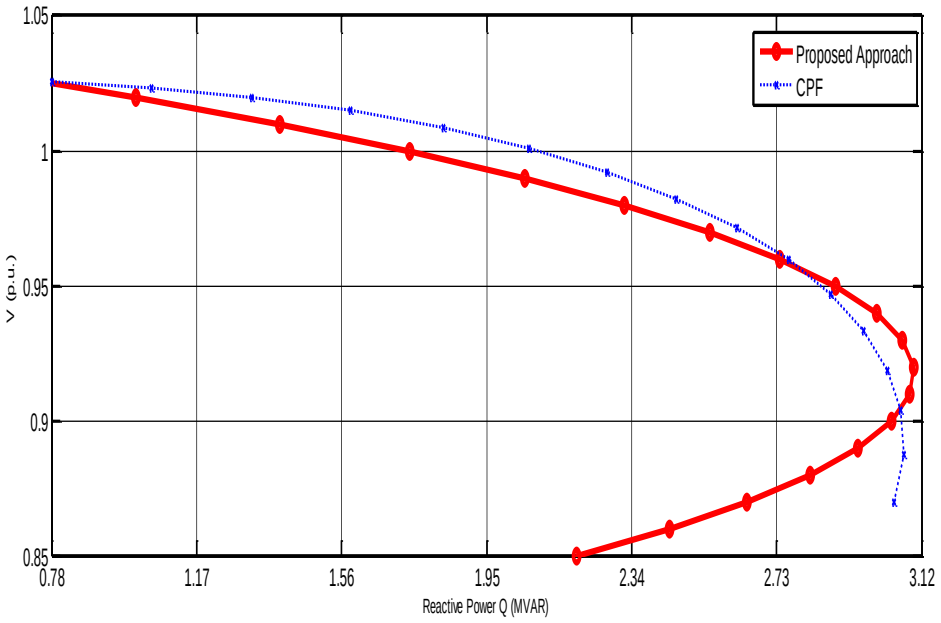

Figure 4.5: *Q-V* curve of critical bus 4 obtained using proposed quadratic curve fitting method and by CPF method for line outage 2-3

4.3.2 New England 39-Bus System

Real power loading margin P_D^{Max} was calculated as per flow chart shown in Fig.4.3 for the system intact case and all the single line outage cases, as in case of IEEE 14-bus system. Phasor measurements are obtained using optimally placed PMUs at bus numbers 4, 8, 12, 16, 18, 20, 23, 25, 26, 27, 29, 30, 31, 32, 33, 34, 35, 36, 37, 38 and 39 (as shown in Table 2.5). Measured voltage magnitude and real power demand of the most critical bus at the three operating points, P_D^{Max} calculated using proposed

approach and real power loadability based most critical bus number have been shown in Table 4.3 for the system intact case and few critical contingency cases. In order to validate real power loadability obtained by proposed approach, real power demand versus voltage magnitude curve (*P*-*V* curve) of most critical bus was plotted using continuation power flow (CPF) method [10] for the system intact case and all the single line outage cases. For obtaining *P*-*V* curve of the most critical bus, its real power demand was varied as per (4.15). Real power loading margin (P_D^{Max}) of the most critical bus obtained by CPF method (real power demand at the nose point of its *P*-*V* curve) have also been shown in Table 4.3 for the system intact case and few critical contingency cases. It is observed from Table 4.3 that real power loading margin obtained by proposed approach closely matches with real power loading margin found by continuation power flow method.

Table 4.3: Real power loading margin under critical contingencies (New England 39-bus system)

C.C.	M.C.B.	Point 1		Point 2		Point 3		P_D^{Max} (MW)	
		V_j^1 (p.u.)	$P_{D_j}^1$ (MW)	V_j^2 (p.u.)	$P_{D_j}^2$ (MW)	V_j^3 (p.u.)	$P_{D_j}^3$ (MW)	P.A.	CPF
Intact	29	1.03	283.5	0.96	1227.56	0.90	1360.80	1363.64	1686.83
28-29	29	1.02	283.5	0.95	768.29	0.89	853.34	856.17	989.42
29-38	20	1.00	680	0.97	2380	0.96	2380	2420.8	2380
21-22	23	1.05	247.5	0.95	868.73	0.91	905.85	908.33	930.60
22-35	29	1.03	283.5	0.98	1097.15	0.96	1097.15	1108.49	1099.98
10-32	29	1.03	283.5	0.98	1102.82	0.96	1102.82	1114.16	1102.82

C.C. = critical contingency, M.C.B. = most critical bus, P.A. = proposed approach

P-V curve of bus 20 (most critical bus) obtained by proposed quadratic fitting of nose curves using PMU measurements/pseudo measurements obtained at three operating points as well as continuation power flow based *P-V* curve of same bus have been shown in Fig.4.6 for the outage of line 29-38. It is observed from Fig.4.6 that nose point real power loadability obtained by proposed approach closely matches with real power loading margin of the bus obtained by continuation power flow method.

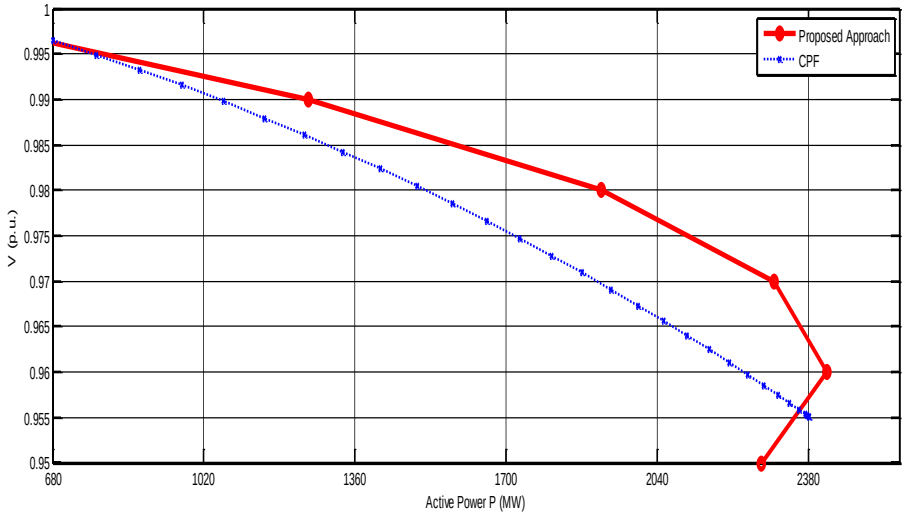

Figure 4.6: *P-V* curve of critical bus 20 obtained using proposed quadratic curve fitting method and by CPF method for line outage 29-38

Reactive power loading margin (Q_D^{Max}) was calculated as per flow chart shown in Fig.3 for the system intact case and all the single line outage cases, as in case of IEEE 14-bus system. In order to validate reactive power loading margin obtained by proposed approach, reactive power demand versus voltage magnitude curve (*Q-V* curve) of the most critical bus was also obtained by CPF method for the system intact case and all the single line outage cases. For obtaining *Q-V* curve of the most critical bus, its reactive power demand was varied as per (4.16). Measured voltage magnitude and reactive power demand of most critical bus at three operating points, reactive

power loading margin (Q_D^{Max}) obtained by proposed approach as well as by CPF method have been shown in Table 4.4, for the system intact case and few critical contingency cases. Reactive power loadability based most critical bus number has also been shown in Table 4.4 for all these cases. It is observed from Table 4.4 that Q_D^{Max} obtained by proposed approach closely matches with Q_D^{Max} obtained by CPF method.

Table 4.4: Reactive power loading margin under critical contingencies (New England 39-bus system)

C.C.	M.C.B.	Point 1		Point 2		Point 3		Q_D^{Max} (MVAR)	
		V_j^1 (p.u.)	$Q_{D_j}^1$ (MVAR)	V_j^2 (p.u.)	$Q_{D_j}^2$ (MVAR)	V_j^3 (p.u.)	$Q_{D_j}^3$ (MVAR)	P.A.	CPF
Intact	29	1.03	25.38	0.96	274.74	0.91	609.12	122.08	151.01
28-29	29	1.02	25.38	0.95	171.95	0.89	381.97	76.65	88.58
29-38	20	1.00	20.6	0.97	180.25	0.96	360.5	73.34	72.10
15-16	15	1.02	30.6	0.96	76.5	0.92	153	142.6	168.9
2-25	25	1.03	9.44	0.95	23.6	0.91	47.2	42.10	51.26
10-32	29	1.03	25.38	0.98	246.82	0.96	493.64	99.74	98.73

C.C. = critical contingency, M.C.B. = most critical bus, P.A. = proposed approach

Q-V curve of bus 29 (most critical bus) obtained by proposed quadratic curve fitting of nose curves using PMU measurements/pseudo measurements at three operating points as well as CPF based *Q-V* curve of same bus have been shown in Fig.4.7 for the outage of line 10-32. It is observed from Fig.4.7 that nose point reactive power loadability of bus 29 obtained by proposed approach closely matches with CPF based nose point reactive power demand.

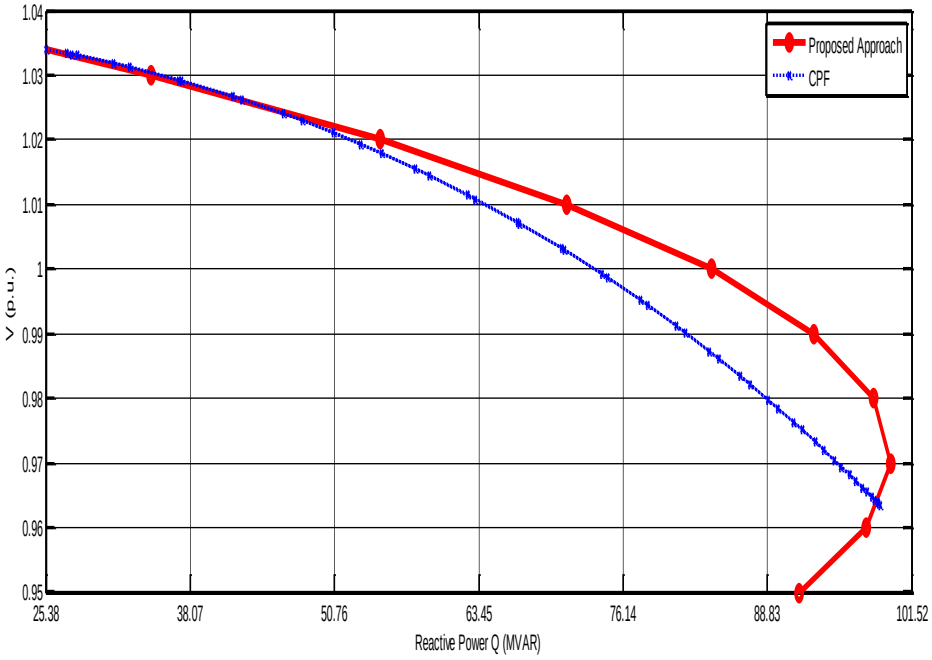

Figure 4.7: *Q-V* curve of critical bus 29 obtained using proposed quadratic curve fitting method and by CPF method for line outage 10-32

4.3.3 NRPG 246-Bus System

Phasor measurements were obtained at regular intervals using optimally placed 97 PMUs shown in Table 2.8.

P_D^{Max} was calculated for the system as per flow chart shown in Fig.4.3 for the system intact case and all the single line outage cases, as in case of IEEE 14-bus

system and New England 39-bus system. Measured voltage magnitude and real power demand of the most critical bus at the three operating points, real power loadability based most critical bus number and P_D^{Max} calculated using proposed approach have been shown in Table 4.5 for the system intact case and few critical contingency cases. In order to validate real power loading margin obtained by proposed approach, real power demand versus voltage magnitude curve (*P*-*V* curve) of most critical bus was plotted using continuation power flow (CPF) method [10] for the system intact case and all the single line outage cases. CPF based *P*-*V* curve was obtained by varying real power demand at the bus as per (4.15). Real power loading margin (P_D^{Max}) of the most critical bus obtained by CPF method (real power demand at the nose point of its *P*-*V* curve) have also been shown in Table 4.5 for the system intact case and few critical contingency cases. It is observed from Table 4.5 that real power loading margin obtained by proposed approach closely matches with real power loading margin found by continuation power flow method.

P-*V* curve of bus 174 (most critical bus) obtained by proposed quadratic fitting of nose curves using PMU measurements/pseudo measurements at three operating points as well as continuation power flow based *P*-*V* curve of same bus have been shown in Fig.4.8 for the outage of line 194-198. It is observed from Fig.4.8 that nose point real power loadability obtained by proposed approach closely matches with real power loading margin of the bus obtained by continuation power flow method.

Q_D^{Max} was calculated for the system intact case and all the single line outage cases, as in case of IEEE 14-bus system and New England 39-bus system. In order to validate reactive power loading margin obtained by proposed approach, reactive power demand

versus voltage magnitude curve (*Q*-*V* curve) of the most critical bus was also obtained by CPF method for the system intact case and all the single line outage cases. CPF based *Q*-*V* curve was obtained by varying reactive power demand at the bus as per (4.16). Measured voltage magnitude and reactive power demand of most critical bus at three operating points, reactive power loading margin (Q_D^{Max}) obtained by proposed approach as well as by CPF method have been shown in Table 4.6, for the system intact case and few critical contingency cases. Reactive power loadability based most critical bus number has also been shown in Table 4.6 for all these cases. It is observed from Table 4.6 that Q_D^{Max} obtained by proposed approach closely matches with Q_D^{Max} obtained by CPF method.

Q-*V* curve of bus 158 (most critical bus) obtained by proposed quadratic curve fitting of nose curves using PMU measurements/pseudo measurements at three operating points as well as CPF based *Q*-*V* curve of same bus have been shown in Fig.4.9 for the outage of line 156-158. It is observed from Fig.4.9 that nose point reactive power loadability of bus 158 obtained by proposed approach closely matches with CPF based nose point reactive power demand.

Table 4.5: Real power loading margin under critical contingencies (NRPG 246-bus system)

C.C.	M.C.B.	Point 1		Point 2		Point 3		P_D^{Max} (MW)	
		V_j^1 (p.u.)	$P_{D_j}^1$ (MW)	V_j^2 (p.u.)	$P_{D_j}^2$ (MW)	V_j^3 (p.u.)	$P_{D_j}^3$ (MW)	P.A.	CPF
Intact	174	1.01	169.8	0.95	419.41	0.90	485.63	487.33	641.84
173-174	174	1.01	169.8	0.96	249.61	0.90	264.89	269.98	344.69
40-41	174	1.01	169.8	0.96	382.05	0.94	384.35	388.84	383.75
166-173	174	1.01	169.8	0.95	339.6	0.90	383.7	385.45	434.69
156-158	158	1.01	174.7	0.97	468.2	0.96	459.46	473.44	476.93
194-198	174	1.01	174.7	0.95	468.2	0.90	459.46	506.63	518.86

C.C. = critical contingency, M.C.B. = most critical bus, P.A. = proposed approach

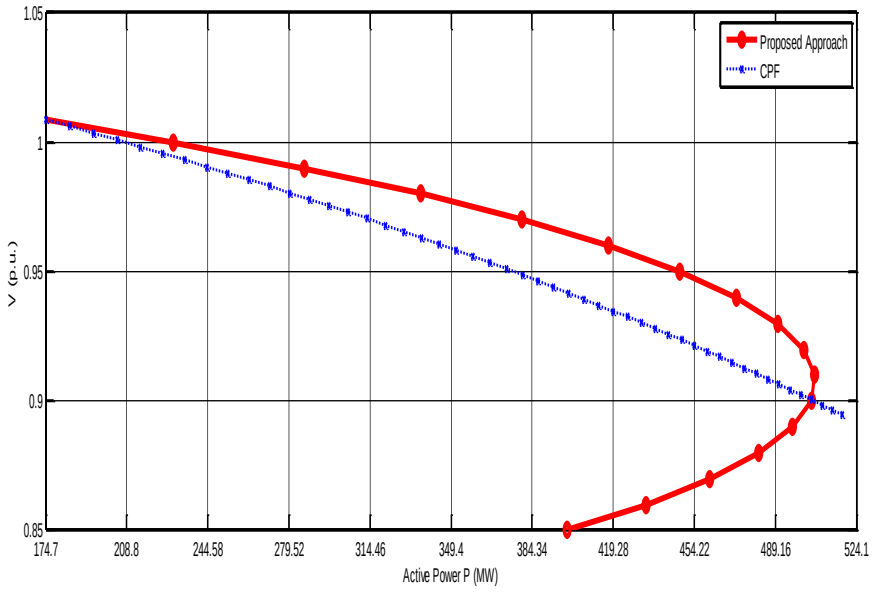

Fig.4.8. *P-V* curve of critical bus 174 obtained using proposed approach and by CPF method for line outage 194-198 (NRPG 246-bus system)

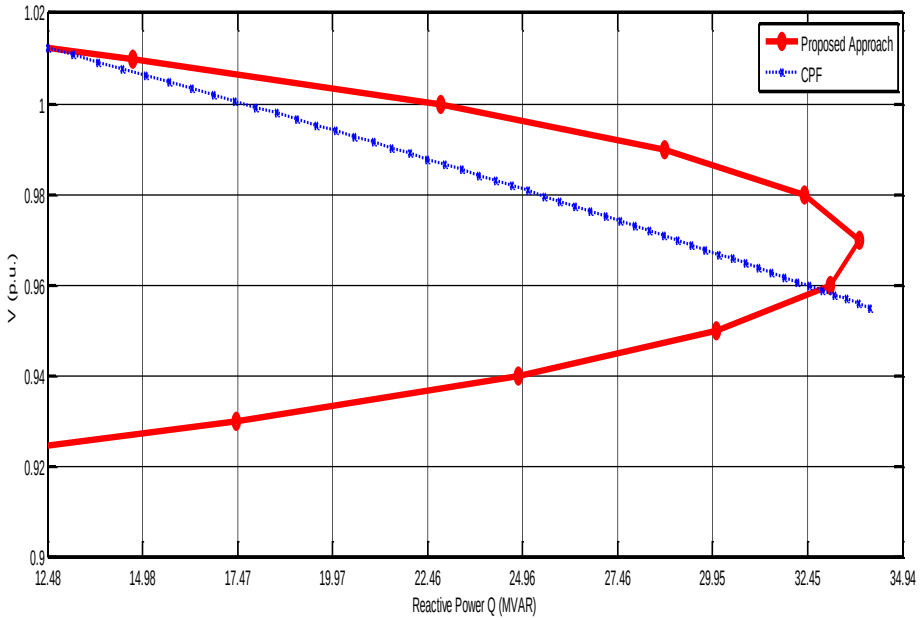

Fig.4.9. *Q-V* curve of critical bus 158 obtained using proposed approach and by CPF method for line outage 156-158 (NRPG 246-bus system)

Table 4.6: Reactive power loading margin under critical contingencies (NRPG 246-bus system)

C.C.	M.C.B.	Point 1		Point 2		Point 3		Q_D^{Max} (MVAR)	
		V_j^1 (p.u.)	$Q_{D_j}^1$ (MVAR)	V_j^2 (p.u.)	$Q_{D_j}^2$ (MVAR)	V_j^3 (p.u.)	$Q_{D_j}^3$ (MVAR)	P.A.	CPF
Intact	174	1.01	13.52	0.95	83.49	0.90	193.34	38.80	51.11
173-174	174	1.01	13.52	0.96	49.69	0.90	105.46	21.50	27.45
40-41	174	1.01	13.52	0.96	76.05	0.94	151.42	30.96	30.56
166-173	174	1.01	13.52	0.95	67.6	0.90	152.8	30.69	34.61
156-158	158	1.01	12.48	0.97	50.86	0.96	164.11	33.82	34.07
63-70	156	1.01	17.74	1.01	44.35	1.01	88.7	19.51	19.33

C.C. = critical contingency, M.C.B. = most critical bus, P.A. = proposed approach

4.4 Conclusions

Online monitoring of voltage stability margin using PMU measurements has been proposed in this chapter. Proposed approach estimates voltage stability margin based on measurements obtained at three operating points. Due to highly dynamic nature of power systems, voltage stability margin keeps on changing. Therefore, proposed approach suggests computation of updated voltage stability margin at regular intervals based on new PMU measurements obtained. Change in operating scenario has been simulated in PSAT software considering different single line outage cases. Accuracy of proposed approach has been validated by comparing voltage stability margin obtained by proposed approach with margin estimated using continuation power flow method under same set of operating conditions. Case studies performed on three test systems show that real power loading margin as well as reactive power loading margin of the system obtained by proposed approach closely matches with loading margin obtained by continuation power flow method.